Nanoscale Advances

ROYAL SOCIETY OF CHEMISTRY

PAPER

View Article Online
View Journal | View Issue

Cite this: *Nanoscale Adv.*, 2022, **4**, 4016

A highly efficient polydopamine encapsulated clinical ICG theranostic nanoplatform for enhanced photothermal therapy of cervical cancer†

Zhong Du,‡[a] Rong Ma,‡[a] Shuang Chen,[a] Huimin Fan,[b] Youqiang Heng,[a] Ting Yan,[b] Gulinigaer Alimu,[b] Lijun Zhu,[b] Xueliang Zhang,[b] Nuernisha Alifu *[b] and Cailing Ma*[a]

Photothermal therapy (PTT) is a safe and efficient anti-tumor treatment. A photothermal agent (PTA) with good biocompatibility and strong photothermal properties is of great importance for PTT. In this study, near-infrared (NIR) excitable clinical indocyanine green (ICG) was utilized as a PTA and further encapsulated by another PTA polydopamine (PDA) to form highly stable and efficient ICG@PDA nanoparticles (NPs). Then the ICG@PDA NPs were modified with methoxy polyethylene glycol amine ($mPEG_{2000}$-NH_2) to form biocompatible ICG@PDA@PEG NPs. ICG@PDA@PEG NPs showed good water solubility and a spherical shape with an average size of 140 nm. Furthermore, the photothermal properties of ICG@PDA@PEG NPs were studied and excellent photothermal performance with a photothermal conversion efficiency of 43.7% under 808 nm laser irradiation was achieved. Then, the PTT properties of ICG@PDA@PEG NPs were confirmed on HeLa cells with an efficiency of 86.1%. Meanwhile, the *in vivo* biocompatibility and toxicity of ICG@PDA@PEG NPs were evaluated. No apparent *in vivo* toxicity was observed in 24 hours and 7 days. Next, *in vivo* PTT analysis was conducted for cervical tumor-bearing nude mice under 808 nm laser excitation. It showed a good anti-tumor effect *in vivo*. Thus, ICG@PDA@PEG NPs exhibited great potential for safe and efficient photothermal therapy in anti-tumor therapy.

Received 30th May 2022
Accepted 10th August 2022

DOI: 10.1039/d2na00341d

rsc.li/nanoscale-advances

Introduction

Cervical cancer is the fourth most common cancer in women and one of the leading causes of cancer death.[1] However, conventional anti-tumor treatment methods such as chemotherapy, radiotherapy, and surgical treatment cause certain damage to the body and may have certain side effects.[2,3] The development of anti-tumor treatment has drawn an upsurge of research all over the world. Among the efficient tumor treatments, photothermal therapy (PTT) is a popular one.[4] Compared with traditional therapy methods, PTT has high therapeutic efficiency and negligible side effects.[5,6]

The PTT process is mainly performed with heat energy, which is generated from photothermal agents (PTAs) under light irradiation and kills tumor cells through thermal apoptosis. It has the advantages of few side effects and a high treatment rate.[7] At present, PTT is applied to *in vitro* and *in vivo* biomedical research.[8–12] With the continuous development of research related to PTT, many PTAs have been developed and studied, including platinum, Au nanoparticles (NPs), $MoSe_2$, indocyanine green (ICG), new indocyanine green (IR820) and so on.[13–17] Although, a variety of PTAs have been utilized, there is still a great demand for photothermal materials with good biosafety and photothermal properties.[18]

Clinical indocyanine green (ICG) is a fluorescence nanoprobe, which has been approved by the United States (US) Food and Drug Administration (FDA).[19,20] ICG has been utilized to detect liver malignancy or vascularization in clinical operation.[21] Besides, ICG is also one of the popular PTAs.[22] However, the poor photothermal stability and short *in vivo* circulation time of ICG limited its further application in biomedical applications.[23] Efforts have been made to overcome this problem. A variety of nanocarriers have been utilized to encapsulate ICG to form NPs, such as BSA@ICG NPs and ICG@PSMA NPs for further application *via* improved stability.[24,25] Polymers are one of the popular nanocarriers for the encapsulation of ICG. Among the existing polymers, polydopamine is a favorable one. Dopamine is an important neurotransmitter in the brain, involved in regulation

[a]*Department of Gynecology, The First Affiliated Hospital of Xinjiang Medical University, State Key Laboratory of Pathogenesis, Prevention and Treatment of High Incidence Diseases in Central Asia, Urumqi 830054, China. E-mail: hymcl@sina.com*
[b]*State Key Laboratory of Pathogenesis, Prevention and Treatment of High Incidence Diseases in Central Asia, School of Medical Engineering and Technology, Xinjiang Medical University, Urumqi, 830011, China. E-mail: nens_xjmu@126.com*

† Electronic supplementary information (ESI) available. See https://doi.org/10.1039/d2na00341d

‡ Co-first authors.

of movement, cognition, emotion, positive reinforcement and other related behaviors.[26] And, it can spontaneously polymerize to form polydopamine (PDA) under alkaline conditions.[27] PDA is also widely used as a PTA because of its good PTT properties.[28–33]

In this work, clinical ICG was utilized as a PTA and further encapsulated by polydopamine (PDA), which is also a PTA to form ICG@PDA nanoparticles (NPs). Then the ICG@PDA NPs were modified with a methoxy polyethylene glycol amine ($mPEG_{2000}$-NH_2) to form ICG@PDA@PEG NPs *via* Michael's addition reaction and the Schiff-base reaction.[34] ICG@PDA@PEG NPs showed good water solubility and a spherical shape with an average size of 140 nm. ICG@PDA@PEG NPs showed excellent photothermal performance with a photothermal conversion efficiency of 43.7% under 808 nm laser irradiation. Furthermore, excellent photothermal stability was confirmed by cold/hot cycle experiments under the same experimental conditions. In addition, cytotoxicity analyses were performed and low cytotoxicity of ICG@PDA@PEG NPs was confirmed. Then, the cellular uptake of ICG@PFA@PEG NPs was analyzed by confocal laser scanning microscopy (CLSM). The PTT properties of ICG@PDA@PEG NPs were confirmed on HeLa cells with an efficiency of 86.1%. Meanwhile, the *in vivo* metabolism and *in vivo* toxicity of ICG@PDA@PEG NPs were studied. No apparent *in vivo* toxicity was observed in 24 h and 7 days. Furthermore, *in vivo* PTT analysis was conducted for cervical tumor-bearing nude mice under near-infrared 808 nm laser irradiation. The temperature of the tumor site exceeded the thermal apoptosis temperature of tumor cells (42 °C) because of the high efficiency of ICG@PDA@PEG NPs.[35] Next, *in vivo* PTT analysis was conducted for the cervical tumor-bearing nude mice under 808 nm laser excitation. It showed a good anti-tumor effect *in vivo*. Furthermore, ICG@PDA@PEG NPs exhibited excellent biocompatibility and good *in vivo* biodistribution with a long *in vivo* circulation time. It was proved that ICG@PDA@PEG has great potential as a photothermal material in antitumor photothermal therapy.

Experimental section

Materials

Clinical indocyanine green (ICG) was purchased from Hangzhou Aoya Biotechnology Co., Ltd. Dopamine hydrochloride was bought from Shanghai Macklin Biochemical Co., Ltd. Methoxy polyethylene glycol amine ($mPEG_{2000}$-NH_2) was purchased from Shanghai Macklin Biochemical Co., Ltd. Tris buffer (hydroxy-methyl) was bought from Shanghai Aladdin Biochemical Technology Co., Ltd. Phosphate-balanced saline (PBS), high glucose Dulbecco's modified essential medium (DMEM), fetal bovine serum (FBS) and trypsin were bought from Shanghai Hyclone Co., Ltd. An Annexin V-FITC apoptosis detection kit was purchased from BD Biosciences Pharmingen Co., Ltd. A Cell Counting Kit-8 (CCK-8), 4′,6-diamidino-2-phenylindole (DAPI), calcein acetomethoxyl ester (calcein AM) and propidium iodide (PI) were bought from Bio-sharp Co., Ltd. Deionized (DI) water was used in all experimental processes.

Cells and animals

The human cervical cancer cell line (HeLa) and cervical epithelial cell line(H8) were obtained from the American Type Culture Collection (ATCC) and cultured in DMEM medium containing 10% FBS and 1% antibiotics (penicillin–streptomycin) placed in a humidified incubator containing 5% CO_2 at 37 °C.

BALB/c mice (female, 18–20 g) and nude mice (female, 18–20 g) were purchased from Beijing Vital River Laboratories and fed in the Animal Experiment Center, Xinjiang Medical University. All animal procedures were approved by the Ethics Committee for Animal Experiments of Xinjiang Medical University. Under the management of the Animal Care and Use Committee of Xinjiang Medical University, all experimental operations met the requirements. All proposals have been submitted and approved. All animal procedures were carried out in accordance with the guidelines for the care and use of experimental animals of the National Institutes of Health and approved by the Animal Care and Use Committee of Xinjiang Medical University (20191113-08).

Preparation of ICG@PDA@PEG NPs

ICG was biochemically modified through the following three steps. Firstly, 1 mg of ICG was dissolved into 1 mL of Tris buffer (pH = 8.5) to make stock solution A. 2.5 mg of dopamine hydrochloride was dissolved into 1 mL of Tris buffer (pH = 8.5) to make stock solution B. Then, 1 mL of stock solution A was added into 1 mL of stock solution B and stirred at a high speed at room temperature for 12 hours. Finally, the ICG@PDA NPs were collected by centrifugation and washed with DI water.

Then, 1 mg of ICG@PDA NPs was dissolved into 1 mL of Tris buffer (pH = 8.5) to make stock solution C. 2 mg of $mPEG_{2000}$-NH_2 was dissolved into 1 mL of Tris buffer (pH = 8.5) to make stock solution D. Then, 1 mL stock solution C was added into 1 mL stock solution D and stirred at a high speed at room temperature for 8 hours. After stirring for 8 hours, the PEGylated ICG@PDA NPs (ICG@PDA@PEG NPs) were collected by centrifugation and washed with DI water three times.

Characterization of ICG@PDA@PEG NPs

The morphology of the ICG@PDA@PEG NPs was characterized by scanning electron microscopy (SEM, JSM-7610FPlus, Japan) and transmission electron microscopy (TEM, JEM-1230, JEOL, Ltd, Japan). The absorption spectra of the ICG, ICG@PDA NPs and ICG@PDA@PEG NPs were obtained from a Lambda 750S UV/vis/NIR spectrophotometer (PerkinElmer). The dynamic diameter and distribution of the ICG@PDA@PEG NPs were characterized by using a Zetasizer Nano ZS-90 (Malvern, UK). The fluorescence spectra of ICG, ICG@PDA NPs and ICG@PDA@PEG NPs were recorded with a Duetta fluorescence and absorbance spectrofluorophotometer (HORIBA Canada). The loading efficiency (LE) of ICG was calculated *via* the UV vis spectrophotometric method.[36] The loaded ICG dose in ICG@PDA@PEG NPs was determined from the absorption value. The calculation formula was as follows (eqn (1)).[36]

$$\text{LE } (\%) = \frac{\text{ICG}_{\text{loaded}}}{\text{weight}_{\text{NPs}}} \times 100\% \quad (1)$$

Evaluation of *in vitro* photothermal performance

The photothermal properties of ICG@PDA@PEG NPs in aqueous dispersion were studied. The temperature change of ICG, PDA NPs, ICG@PDA NPs and ICG@PDA@PEG NPs was analyzed under 808 nm laser irradiation (0.8 W cm^{-2}) for 15 minutes.

Then, to further analyze the photothermal properties of ICG@PDA@PEG NPs, five different concentrations (12.5, 25, 50, 100 and 125) (μg mL^{-1}) of ICG@PDA@PEG NPs in aqueous dispersion were observed under 808 nm laser irradiation (0.8 W cm^{-2}) for 15 minutes.

Next, 125 μg mL^{-1} of ICG@PDA@PEG NPs in aqueous dispersion were exposed to 808 nm laser irradiation at different power densities (0.4, 0.6, 0.8 and 1.0 W cm^{-2}) for 15 minutes. The temperature of the samples was calculated by using an infrared thermal imaging camera (FOTRIC, Shanghai Heat Image Technology Co., Ltd).

Finally, the photostability of the ICG@PDA@PEG NPs was evaluated. 125 μg mL^{-1} of ICG@PDA@PEG NPs in aqueous dispersion were irradiated under an 808 nm laser (0.8 W cm^{-2}) for 15 minutes and then cooled to room temperature. To evaluate the photothermal conversion efficiency of ICG@PDA@PEG NPs, 125 μg mL^{-1} of ICG@PDA@PEG NPs in aqueous dispersion were exposed to 808 nm laser irradiation (0.8 W cm^{-2}) for 15 minutes and then cooled to room temperature. The photothermal conversion efficiency (η) of ICG, PDA and ICG@PDA@PEG NPs was calculated according to the following equation (eqn (2)).[24,37]

$$\eta = \frac{M_{\text{D}} C_{\text{D}} (T_{\max} - T_{\max,\text{water}})}{\tau_{\text{s}} I \left(1 - 10^{-A_{808}}\right)} \times 100\% \quad (2)$$

(M_{D}) and (C_{D}) are the mass and heat capacity of deionized water, $T_{\max}$ and $T_{\max,\text{water}}$ are the maximum equilibrium temperature of NPs solution and water, τ_{s} is the system time constant, I is the NIR laser power, and A_{808} represents the dispersion absorptivity at 808 nm.

Cellular uptake

The fluorescence of ICG@PDA@PEG NPs was observed, and then the cell uptake ability of ICG@PDA@PEG NPs on HeLa cells was studied by using a confocal laser scanning microscope (CLSM, Nikon ECLIPSE Ti, Japan). 1 × 10^5 HeLa cells were cultured in a confocal culture dish (35 mm in diameter). ICG@PDA@PEG NPs were dissolved in DMEM medium to form a concentration of 125 μg mL^{-1}, and then the medium was incubated with HeLa cells for 2 hours.

After incubation, the HeLa cells were washed with 1× PBS three times and stained with DAPI for 10 minutes and then washed with 1× PBS three times. Finally, the cells were observed by CLSM.

Cytotoxicity analysis

Cytotoxicity analysis was performed by using CCK-8. HeLa cells were planted in 96-well plates, in which each well of the experimental group contained 5 × 10^3 cells and 200 μL of medium and incubated for 24 hours. ICG, ICG@PDA NPs, and ICG@PDA@PEG NPs were dissolved in DMEM mediums to form different concentrations (0, 6.25, 12.5, 25, 50, 100 and 200) (μg mL^{-1}), and then the different concentrations of mediums were incubated with HeLa cells for 24 hours. After 24 hours of incubation, the cell survival rate was calculated by the CCK-8 standard method.

Then, H8 cells were planted in 96-well plates (the same as before). ICG@PDA@PEG NPs were dissolved in DMEM mediums with different concentrations (0, 6.25, 12.5, 25, 50, 100 and 200) (μg mL^{-1}), and then incubated with H8 cells for 24 hours. After 24 hours of incubation, the cell survival rate was calculated by the CCK-8 standard method.

Finally, HeLa cells were planted in 96-well plates (the same as before). ICG@PDA@PEG NPs were dissolved in DMEM mediums with different concentrations (the same as before) and then incubated with HeLa cells for 24 hours. After 24 hours of incubation, HeLa cells were irradiated with an 808 nm laser (0.8 W cm^{-2}) for 15 minutes. After irradiation, the cell survival rate was calculated by the CCK-8 standard method.

Evaluation of the photothermal effect *in vitro*

To evaluate the photothermal effect of ICG@PDA@PEG on HeLa cells, 4 different groups were used to evaluate the photothermal effect of ICG@PDA@PEG NPs on HeLa cells under different conditions.

At First, 4 × 10^5 HeLa cells were planted in 4 confocal dishes with 1 × 10^5 cells in each dish, and then cultured for 12 hours. The 4 dishes were labeled group A, group B, group C and group D, respectively. Group A was the control group. The medium in group B dishes needed to be replaced with a newly configured medium, which containing ICG@PDA@PEG NPs. Then, ICG@PDA@PEG NPs was dissolved in DMEM medium to form a concentration of 125 μg mL^{-1}. Next, the old medium was replaced with a newly configured medium containing ICG@PDA@PEG NPs. After that, the cells were incubated for 2 hours. Group C was the one which only received 808 nm laser irradiation (0.8 W cm^{-2}) for 15 minutes. The medium in the culture dish of group D needed to be replaced with a newly configured medium (the same as group B) and then incubated for 2 hours. After incubation, group D was irradiated with an 808 nm laser for 15 minutes. Then, HeLa cells were treated in the 4 groups with calcein AM and PI for 20 minutes. Finally, the 4 groups were observed by CLSM. Under the excitation of two different wavelengths of 490 nm and 545 nm, the fluorescence images of HeLa cells were collected through green (calcein AM) and red (PI) channels and detected by the excitation light emission of 810–1000 nm respectively.

In addition, the photothermal treatment of ICG@PDA@PEG NPs in HeLa cells was evaluated by flow cytometry. 4 identical 6-well plates were prepared. Then, HeLa cells were planted in 6-well plates, each containing 3 × 10^5 HeLa cells, and incubated

for 24 hours. The 4 identical 6-well plates were labeled group A, group B, group C and group D. Group A was the control group (no intervention). The medium in group B dishes needed to be replaced with a newly configured medium, which containing a concentration of 125 μg mL^{-1} ICG@PDA@PEG NPs and then incubated for 2 hours. Group C was the group which only received 808 nm laser irradiation (0.8 W cm^{-2}) for 15 minutes. The medium in the culture dish of group D needed to be replaced with a newly configured medium (the same as group B) and then incubated for 2 hours. After incubation, group D was irradiated with an 808 nm laser for 15 minutes. Finally, HeLa cells in the four groups were washed with 1× PBS, digested with trypsin, and collected by centrifugation. The collected cells were washed twice with 1× PBS and mixed with 0.5 mL of annexin binding buffer. PI and annexin V-FITC containing binding buffer were added to the cell suspension and stained for 15 minutes. Finally, the four groups were analyzed by flow cytometry (BD LSRII, FACS Calibur).

Evaluation of *in vivo* photothermal therapy on cervical tumor-bearing nude mice

A subcutaneous cervical tumour-bearing nude mice model was established and utilized for the evaluation of *in vivo* PTT. BALB/c nude mice (female, 18–20 g) were utilized for the establishment of the cervical tumor model. 1×10^7 HeLa cells were injected into the lower right side of the mouse back through a 1 mL syringe. When the subcutaneous tumor volume reached 50 mm^3, two groups of cervical tumour-bearing nude mice were selected to evaluate *in vivo* photothermal properties. One of the groups was selected to inject ICG@PDA@PEG NPs (1.5 mg kg^{-1}) into the tumor site, and then irradiated with an 808 laser for 10 minutes. In the other group, 50 μL of 1× PBS was injected into the tumor, and then irradiated with an 808 laser for 10 minutes. Finally, the temperature changes of subcutaneous tumor sites in the two groups were compared by using an infrared thermal imaging camera.

Then, sixteen of the cervical tumour-bearing nude mice were selected to evaluate the effect of *in vivo* photothermal therapy. These mice were randomly divided into four groups ($n = 4$ per group) as follows: (1) control; (2) ICG@PDA@PEG NPs only; (3) laser only; (4) ICG@PDA@PEG NPs + laser. The mice in the control group were injected with 50 μL of 1× PBS into the tumor. The mice in the ICG@PDA@PEG NPs only group were injected with ICG@PDA@PEG NPs (1.5 mg kg^{-1}) into the tumor site of the mice. The mice in the laser group were irradiated with an 808 nm laser (0.8 W cm^{-2}) for 10 minutes. The mice in the ICG@PDA@PEG NPs + laser group were selected to inject ICG@PDA@PEG NPs (1.5 mg kg^{-1}) into the tumor site of the mice, and then irradiated with an 808 nm laser (0.8 W cm^{-2}) for 10 minutes. The changes of the tumor size and body weight of each group of mice were recorded. After 11 days, the mice were dissected, and the main organs of mice, heart, liver, spleen, lung and kidney, were taken and stained with hematoxylin–eosin staining (H&E). Finally, these sections were observed and analyzed by using an inverted digital microscope (Leica).

Biosafety assessment

The toxicity of ICG@PDA@PEG NPs in the main organs of mice was analyzed. ICG@PDA@PEG NPs (1.5 mg kg^{-1}) were injected into the tail vein of mice, and then the mice were dissected 24 hours and 7 days later. The main organs of mice, heart, liver, spleen, lung and kidney, were taken and stained with H&E. Finally, these sections were observed and analyzed with an inverted digital microscope (Leica).

In vivo metabolism analysis

The metabolism of ICG@PDA@PEG NPs in nude mice was realized by using an *in vivo* fluorescence imaging system (745 nm laser excitation and 840 nm emission). Four groups of nude mice were prepared ($n = 3$ for each group). Group A was the control group, and nude mice were injected with 200 μL of 1× PBS through the tail vein. In group B, nude mice were injected with ICG (1.5 mg kg^{-1}) through the tail vein. In group C, nude mice were injected with ICG@PDA NPs (1.5 mg kg^{-1}) through the tail vein. In group D, nude mice were injected with ICG@PDA@PEG NPs (1.5 mg kg^{-1}) through the tail vein. After injection into the tail vein, the nude mice were selected for *in vivo* fluorescence analysis at 2 hours, 8 hours, 24 hours, 48 hours, and 72 hours. After 72 hours, the mice were dissected, and the heart, liver, spleen, lung, kidney, and small intestine of the mice were analyzed through fluorescence.

Statistical analysis

Data are expressed as mean ± standard deviation (SD). The statistical significance was evaluated by a Man–Whitney-*U*-test performed using Origin 9.1 software (OriginLab, Northampton, USA). *P* values < 0.05 were considered statistically significant. (NS, no significance, $*p < 0.05$, $**p < 0.01$, $***p < 0.001$, and $****p < 0.0001$).

Results and discussion

Preparation and characterization of ICG@PDA@PEG NPs

The preparation of ICG@PDA@PEG NPs was mainly based on the polymerization of dopamine hydrochloride into PDA under alkaline conditions.[27] In Tris buffer (pH = 8.5), when dopamine polymerizes into PDA, ICG could be encapsulated into the

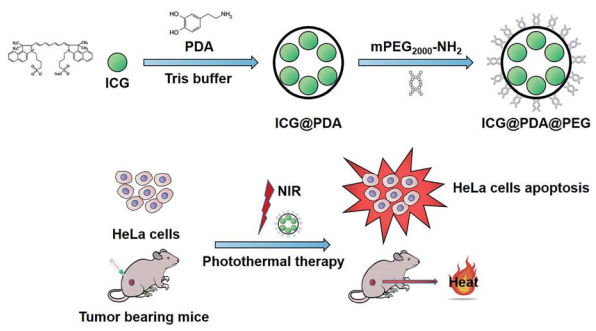

Scheme 1 Schematic illustration of the synthesis process ICG@PDA@PEG NPs and the PTT effect.

polymer matrix ICG@PDA NPs. Then, to improve the biological stability and biosafety of ICG@PDA NPs, ICG@PDA NPs were PEGylated with $mPEG_{2000}$-NH_2, which was also in Tris buffer (pH = 8.5). Finally, ICG@PDA@PEG NPs were purified by centrifugation (Scheme 1). As shown in Fig. 1A, ICG solution (125 μg mL^{-1}, dissolved in DI water) is bright green, while ICG@PDA NPs and ICG@PDA@PEG NPs solutions (125 μg mL^{-1}, dissolved in DI water) were dark green, which is because the PDA has a black color.[38] They are both clear and transparent.

As shown in the TEM image (Fig. 1B) and SEM image (Fig. 1C), the synthesized ICG@PDA@PEG NPs were spherical in shape with an average particle size of 140 nm. Meanwhile, DLS analysis could determine that the average particle size is 140 nm (Fig. 1D). The absorption spectra of ICG NPs, ICG@PDA NPs and ICG@PDA@PEG NPs in aqueous dispersion were characterized. As shown in Fig. 1E, ICG (black line), ICG@PDA NPs (blue line) and ICG@PDA@PEG NPs (red line) had strong absorption peaks at 780 nm. The free ICG NPs in the aqueous dispersion showed two characteristic absorption peaks at 720 nm and 780 nm, which were also visible on the absorption curves of ICG@PDA NPs and ICG@PDA@PEG NPs in the aqueous dispersion. It was proved that ICG, PDA and $mPEG_{2000}$-NH_2 were successfully combined. Then, the fluorescence spectra of ICG, ICG@PDA NPs and ICG@PDA@PEG NPs in aqueous dispersion were studied. As shown in Fig. 1F, ICG (black line), ICG@PDA NPs (blue line) and ICG@PDA@PEG NPs (red line) had peaks in the near-infrared band at 530–540 nm and produced near-infrared fluorescence signals. The fluorescence signals of ICG@PDA NPs and ICG@PDA@PEG NPs were weaker than those of ICG, and the results were attributed to PDA as a colored PTA. Through the intermolecular interaction between ICG and PDA, the fluorescence signal of ICG was affected by the outer PDA, resulting in the weakening of the fluorescence signal of ICG@PDA NPs and ICG@PDA@PEG NPs. Therefore, it was confirmed that ICG@PDA NPs and ICG@PDA@PEG NPs had a morphological structure with PDA as the outer material and ICG coated on it. Finally, the LE of ICG in ICG@PDA@PEG NPs was calculated to be 16.97%. The LE of ICG@PDA@PEG NPs was comparable with that of other different types of polymer encapsulated ICG nanoparticles, such as H-PMOF (17.4%)[39] and Lipo/pB-DOX/ICG (6.0 ± 0.3%).[40]

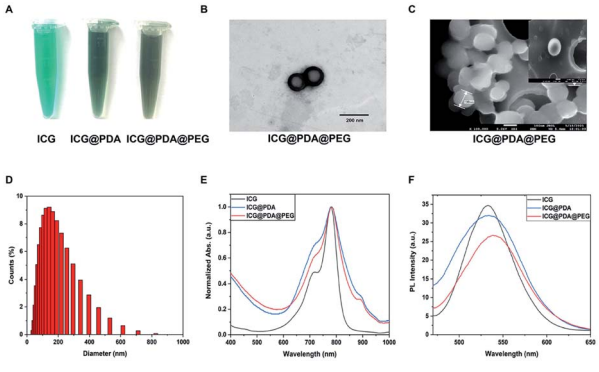

Fig. 1 (A) ICG, ICG@PDA NPs and ICG@PDA@PEG NPs in aqueous dispersion (concentration: 125 μg mL^{-1}). (B) TEM image of ICG@PDA@PEG NPs (scale: 200 nm). (C) SEM image of ICG@PDA@PEG NPs (scale: 100 nm). (D) DLS characterization of ICG@PDA@PEG NPs in aqueous dispersion. (E) The absorption spectra of ICG (black line), ICG@PDA NPs (blue line) and ICG@PDA@PEG NPs (red line) in aqueous dispersion. (F) The fluorescence spectra of ICG (black line), ICG@PDA NPs (blue line) and ICG@PDA@PEG NPs (red line) in aqueous dispersion.

Evaluation of photothermal performance

ICG@PDA@PEG NPs were prepared based on PDA and ICG. The combination of the two PTAs made the synthesized ICG@PDA@PEG NPs had enhanced photothermal properties. The photothermal properties of ICG, PDA NPs, ICG@PDA NPs and ICG@PDA@PEG NPs at the same concentration (125 μg mL^{-1}) were compared under the same 808 nm laser irradiation (0.8 W cm^{-2}) for 15 minutes. As shown in Fig. 2A, the results showed that after laser irradiation, the temperature of ICG@PDA@PEG NP solution increased by 28.8 °C, while that of ICG solution increased by only 21 °C. It was proved that ICG@PDA@PEG NPs had better photothermal properties than ICG. Its excellent photothermal properties lay the foundation for the subsequent evaluation of *in vivo* photothermal properties.

Then, as shown in Fig. 2B, the temperature changes of ICG@PDA@PEG NPs in aqueous dispersion at different concentrations (12.5, 25, 50, 100 and 125) (μg mL^{-1}) were monitored under 808 laser irradiation for 15 minutes. The results showed that with the increase of concentration (ICG@PDA@PEG NPs), the speed and degree of temperature increased continuously. It was confirmed that the photothermal properties of ICG@PDA@PEG NPs were concentration dependent. As shown in Fig. 2C, the temperature changes of ICG@PDA@PEG NPs in aqueous dispersion were monitored and recorded by using an infrared thermal imaging camera. Next, the effects of different laser power densities (0.4, 0.6, 0.8

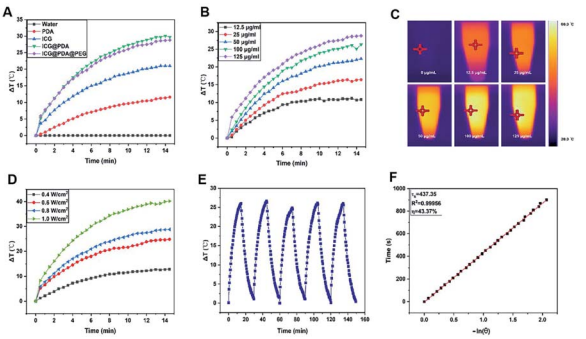

Fig. 2 (A) Temperature changes of different samples (water, PDA, ICG, ICG@PDA NPs, and ICG@PDA@PEG NPs) under 808 nm laser irradiation (125 μg mL^{-1}). (B) The temperature changes of different concentrations (12.5, 25, 50, 100 and 125) (μg mL^{-1}) of ICG@PDA@PEG NPs in aqueous dispersion under 808 nm laser irradiation. (C) The thermal images of ICG@PDA@PEG NPs with different concentrations. (D) Temperature changes of ICG@PDA@PEG NPs with the same concentration (125 μg mL^{-1}) under 808 nm laser irradiation with different power densities (0.4, 0.6, 0.8 and 1) (W cm^{-2}). (E) Temperature change of ICG@PDA@PEG NPs during 5 cold and hot cycles. (F) Linear fitting of time data *versus* $-\ln\theta$ obtained from the cooling period. (NIR laser was 808 nm, 0.8 W cm^{-2}).

and 1.0) (W cm^{-2}) on the photothermal properties of ICG@PDA@PEG NPs were observed. With the increase of laser power density, the photothermal performance of ICG@PDA@PEG NPs is continuously enhanced (Fig. 2D). To evaluate the photostability of the ICG@PDA@PEG NPs, 125 μg mL^{-1} of ICG@PDA@PEG NPs in aqueous dispersion were exposed to 808 nm laser irradiation (0.8 W cm^{-2}) for 15 minutes, and then cooled to room temperature for 5 cycles. During the whole process, there was no significant difference in the temperature change of each cycle, which showed that ICG@PDA@PEG NPs had good photothermal stability as a PTA (Fig. 2E). Finally, as shown in Fig. 2F, the photothermal conversion efficiency of ICG@PDA@PEG NPs was calculated from the change of the temperature of the first cycle in the cold thermal cycle. The time constant of system heat transfer is determined to be τ_s = 437.35 s. According to eqn (2), the η of ICG@PDA @PEG was calculated to be 43.37%, which was comparable to the η of nanoparticles encapsulated with other different types of polymers, such as MINPs (35%)[41] and mPEG-ACA-ICG (20.81%),[42] higher than that of ICG NPs (15.28%) (Fig. S1A†) and PDA NPs (38.99%) (Fig. S1B†).

Cellular uptake

In order to detect the cellular uptake ability, HeLa cells were selected as the experimental object. HeLa cells were incubated with ICG@PDA@PEG NPs (125 μg mL^{-1}) for 2 hours. As shown in Fig. 3A, blue light from DAPI and red light from ICG could be detected. The blue fluorescence of DAPI is excited by a laser at 405 nm, and the red fluorescence of ICG is excited by a laser at 640 nm. It was proved that ICG@PDA@PEG NPs had good biocompatibility and could be taken up by HeLa cells. It could lay the foundation for the subsequent cellular photothermal therapy.

Cytotoxicity analysis

The biosafety of ICG@PDA@PEG NPs was analyzed by the CCK-8 experiment. The results showed that when ICG@PDA@PEG NPs were incubated with HeLa cells for 24 hours, more than 80% of HeLa cells survived even if the concentration of ICG@PDA@PEG NPs reached 100 μg mL^{-1} (Fig. 3B). Next, the cytotoxicity of ICG@PDA@PEG NPs on normal cervical epithelial cells was evaluated (Fig. S2A†). The results were similar to the cytotoxicity of ICG@PDA@PEG NPs on HeLa cells. When the concentration was 100 μg mL^{-1}, the H8 cells still maintained 80% cell activity. Finally, the phototoxicity of ICG@PDA@PEG NPs on HeLa cells was evaluated (Fig. S2B†). The results showed that when the concentration of ICG@PDA@PEG NPs reached 100 μg mL^{-1}, the cellular activity of HeLa cells decreased to less than 20% under 808 nm laser irradiation (0.8 W cm^{-2}). The results confirmed that ICG@PDA@PEG NPs had good photothermal therapeutic properties and could maintain low toxicity to cells. After laser irradiation, they could produce enhanced heat energy and induce a large amount of apoptosis of tumor cells.

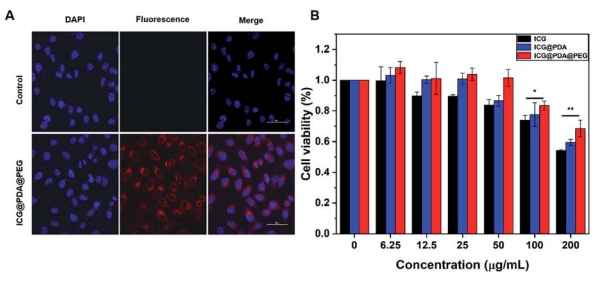

Fig. 3 (A) Confocal laser scanning microscopy (CLSM) fluorescence images of HeLa cells incubated with or without ICG@PDA@PEG NPs. Scale bar: 50 mm. λ_{em} = 800–1000 nm, λ_{ex} = 405 nm (DAPI), and λ_{ex} = 640 nm (ICG). Scale bar: 50 mm. (B) Cell viability of HeLa cells incubated with different concentrations of ICG, ICG@PDA NPs and ICG@PDA@PEG NPs for 24 hours (the data are shown as mean ± SD. n = 3 per group, NS, no significance, *p < 0.05, and **p < 0.01).

Cellular photothermal evaluation

The photothermal therapeutic effect of ICG@PDA@PEG NPs was evaluated by using HeLa cells. Under the observation of CLSM, it could be seen that in group A (control group), where living cells were stained with calcein AM, there were no dead cells (stained with PI). In addition, there were almost no stained dead cells in group B (only ICG@PDA@PEG NPs) and group C (only 808 nm laser irradiation). In group D (ICG@PDA@PEG NPs with 808 nm laser irradiation), almost all HeLa cells were dead and stained with PI.

Meanwhile, flow cytometry was performed to verify the photothermal therapeutic ability of ICG@PDA@PEG NPs. As shown in Fig. 4B, only a small amount of apoptosis occurred in Q_2 and Q_3 quadrants in group B (ICG@PDA@PEG NPs only) and group C (808 nm laser irradiation only). In group D, there was a large amount of apoptosis in Q_2 and Q_3 quadrants, and the total was 85.2%. About 58.4% of the cells showed early apoptosis in the Q_3 quadrant. In conclusion, these results confirmed that ICG@PDA@PEG NPs, as a PTA, not only had

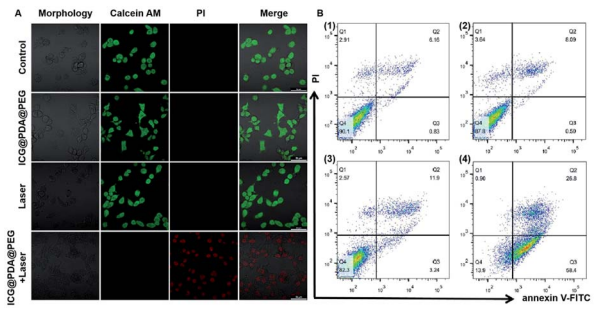

Fig. 4 (A) Confocal laser scanning microscopy (CLSM) images of HeLa cells, control group (no intervention), laser irradiation only group (808 nm laser irradiation at a power density of 0.8 W cm^{-2} for 15 minutes) and ICG@PDA@PEG NPs (125 μg mL^{-1}) and ICG@PDA@PEG NPs (125 μg mL^{-1}) plus laser irradiation (808 nm laser irradiation at a power density of 0.8 W cm^{-2} for 15 minutes) after calcein AM and PI staining. Scale bar: 50 mm. λ_{ex} = 490 nm (calcein AM) and λ_{ex} = 545 nm (PI). (B) Annexin V-FITC and PI staining flow cytometry analysis: (1) control group, (2) laser irradiation only, (3) ICG@PDA@PEG NPs, and (4) ICG@PDA@PEG NPs and laser irradiation.

biological safety, but also had strong photothermal therapeutic ability under 808 nm laser irradiation. These results could lay the foundation for the subsequent animal photothermal experiments.

In vivo photothermal therapy evaluation

Firstly, in order to evaluate the *in vivo* photothermal ability of ICG@PDA@PEG NPs, cervical tumor-bearing mice were selected as our experimental subjects. When the NPs were delivered to the tumor through intravenous or oral administration, only about 0.7% could reach the tumor site.[43] In order to ensure that the ICG@PDA@PEG NPs can totally enter the tumor tissue, the cervical tumor-bearing mice were injected *via* intratumoral injection. Then, ICG@PDA@PEG NPs (1.5 mg kg^{-1}) were injected into the tumor site and irradiated with an 808 nm laser (0.8 W cm^{-2}) for 10 minutes (Fig. 5A). In the control group, as shown in Fig. 5B, 50 μL of 1× PBS was injected into the tumor. After laser irradiation, the temperature of the tumor site increased only 3.2 °C for 10 minutes. As for the ICG@PDA@PEG NPs group, the temperature of the tumor site increased by 15.5 °C to 54 °C. It was proved that ICG@PDA@PEG NPs, as a PTA, could release heat energy at the tumor site under laser irradiation to reach the temperature of killing tumor cells. It could be used as a promising PTA for anti-cervical cancer photothermal therapy. The changes of tumor temperature in mice were observed with an infrared thermal imaging camera (Fig. 5C).

Then, the *in vivo* photothermal therapeutic effect of ICG@PDA@PEG NPs was evaluated by using tumor-bearing nude mice. As shown in Fig. 6A and B, the tumor volume and weight of the four groups of tumor-bearing mice showed different results after different interventions. As shown in Fig. 6C, during the 11 days of observation, the tumor volume of mice in the control group showed a significant increasing trend, and the tumor volume of mice in the ICG@PDA@PEG NPs only

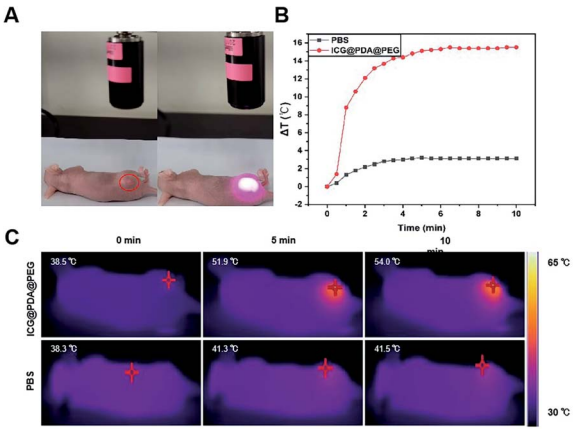

Fig. 5 (A) Images of tumor-bearing mice injected with ICG@PDA@PEG NPs under 808 nm laser irradiation (0.8 W cm^{-2}) for 10 minutes. (B) The temperature changes of tumor sites in the control group (injected with PBS) and ICG@PDA@PEG NPs group during laser irradiation. (C) Thermal images of the temperature change of the tumor site treated with ICG@PDA@PEG NPs.

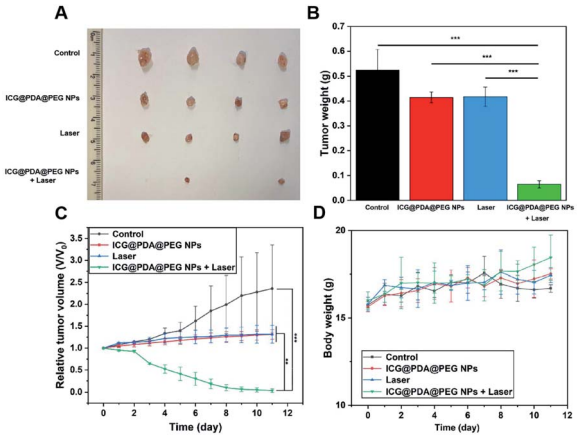

Fig. 6 (A) Pictures of tumor from the mice in each group treated with different interventions after 11 days. (B) Tumor weight of each group at the end of the observation period. Data were displayed as the mean ± SD ($n = 4$ per group, NS, no significance, and ***$p < 0.001$). (C) The relative cancer volume changes in 11 days. Data were displayed as mean ± SD ($n = 4$ per group, NS, no significance, **$p < 0.01$, and ***$p < 0.001$). (D) Changes in the body weight of mice in each group within 11 days.

group and laser group also showed an increasing trend. The tumor volume of mice in the ICG@PDA@PEG NPs + laser group showed a decreasing trend. During the 11 day observation period, there was no significant downward trend in the weight of mice in each group (Fig. 6D).

At the end of the observation period, the main organs of the mice were removed and sectioned and then stained with H&E (Fig. S3†). No obvious tissue damage and necrosis were observed in the section. It was proved that ICG@PDA@PEG NPs had good photothermal therapeutic ability and biological safety. After 808 laser irradiation, it could induce tumor cell apoptosis and inhibit the growth of tumor tissue. After PTT treatment, there was no obvious tissue and organ damage, which had biological safety.

Biosafety assessment

In vivo toxicity was evaluated using BALB/c mice. ICG@PDA@PEG NPs (1.5 mg kg^{-1}) were injected through the tail vein of mice. The main organs of mice were taken out at 24 hours and 7 days to analyze whether the ICG@PDA@PEG NPs caused damage to the body of mice. As shown in Fig. 7, no obvious drug toxicity injury or inflammatory lesions were found in the heart, liver, spleen, lung and kidney of mice in 24 hours or 7 days. It was proved that ICG@PDA@PEG NPs would not cause damage to mice after entering the mice, and ICG@PDA@PEG NPs could be used as a biosafety PTA for photothermal treatment of cervical cancer.

In vivo biodistribution analysis

The stability of ICG@PDA@PEG NPs was greatly enhanced after modification with $mPEG_{2000}$-NH_2. *In vivo* NIR fluorescence imaging at different times within 72 hours was performed by using a small animal *in vivo* imager Interactive Video

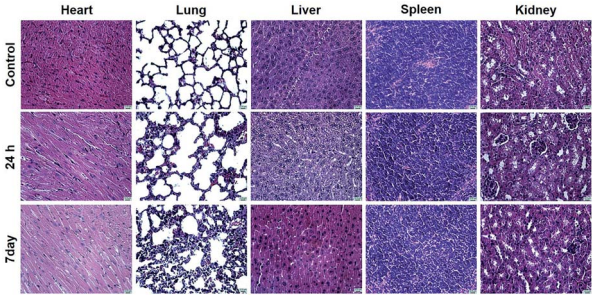

Fig. 7 Histological analysis of the major organs (heart, liver, spleen, lung, and kidney) of mice 24 hours and 7 days after the injection of ICG@PDA@PEG NPs (1.5 mg kg^{-1}). Scale bar: 12.5 μm.

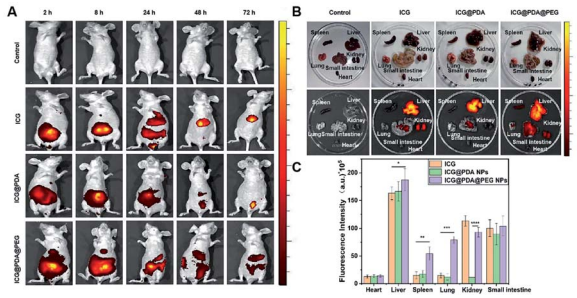

Fig. 8 (A) NIR fluorescence images of nude mice injected with PBS, ICG (1.5 mg kg^{-1}), ICG@PDA NPs (1.5 mg kg^{-1}) and ICG@PDA@PEG NPs (1.5 mg kg^{-1}) through the tail vein at 2 hours, 8 hours, 24 hours, 48 hours and 72 hours. (B) Bright field images and NIR fluorescence images of the dissected organs of mice at 72 hours. (C) Fluorescence intensity analysis of ICG, ICG@PDA NPs and ICG@PDA@PEG NPs in the dissected organs of mice at 72 hours. Data were displayed as mean ± SD ($n = 3$ per group, NS, no significance, *$p < 0.05$, **$p < 0.01$, ***$p < 0.001$, and ****$p < 0.0001$).

Information System (IVIS). The nude mice were divided into 4 groups: control group (injected with PBS), ICG group (1.5 mg kg^{-1}), ICG@PDA NPs group (1.5 mg kg^{-1}) and ICG@PDA@PEG NPs (1.5 mg kg^{-1}) group (Fig. 8A). The fluorescence intensity from the mice treated with ICG@PDA@PEG NPs could remain at least for 72 hours. After 72 hours, the heart, liver, spleen, lung, kidney, and intestine of mice were taken out for analysis (Fig. 8B). Strong fluorescence intensity could be observed from the liver and small intestine of the mice treated with NPs. The fluorescence intensity from the group of the mice treated with ICG@PDA@PEG NPs was higher than that of other groups (Fig. 8C). The results showed that after 72 hours of *in vivo* circulation, ICG@PDA@PEG NPs could still produce fluorescence signals stronger than ICG, indicating that ICG@PDA@PEG NPs had better biological stability than ICG.

Conclusions

In this work, clinical ICG was utilized as a PTA and further encapsulated with PDA. Then the ICG@PDA NPs were further modified with $mPEG_{2000}$-NH_2 to form highly stable and biocompatible ICG@PDA@PEG NPs. ICG@PDA@PEG NPs showed excellent photothermal performance with a photothermal conversion efficiency of 43.7% under 808 nm laser irradiation. Through CLSM, it could be seen that ICG@PDA@PEG NPs could be taken up by HeLa cells and produced fluorescence in cells. Cytotoxicity analysis verified that ICG@PDA@PEG NPs had low cytotoxicity. Under 808 nm laser irradiation, the PTT properties of ICG@PDA@PEG NPs were confirmed on HeLa cells with an efficiency of 86.1%. Meanwhile, *in vivo* biocompatibility and toxicity confirmed that ICG@PDA@PEG NPs had biological safety and biological stability. No apparent *in vivo* toxicity was observed in 24 hours and 7 days. Furthermore, *in vivo* PTT analysis was conducted for cervical tumor-bearing nude mice under near-infrared 808 nm laser excitation. After the combined intervention of ICG@PDA@PEG NPs and 808 nm laser irradiation, the tumors of mice were significantly reduced. It is proved that ICG@PDA@PEG has great potential for safe and efficient photothermal therapy in anti-tumor therapy, which can provide a good foundation in future photothermal research and has a strong future development prospect.

Author contributions

The authors declare competing financial interests.

Conflicts of interest

There are no conflicts to declare.

Acknowledgements

This research was funded by the Natural Science Foundation of Xinjiang Uygur Autonomous Region (No. 2020D01C151), National Natural Science Foundation of China (No. 82060326 and 62035011), Fundamental Research Funds for the Central Universities and State Key Laboratory of Pathogenesis, Prevention and Treatment of High Incidence Diseases in Central Asia Fund (No. SKL-HIDCA-2020-6, SKL-HIDCA-2021-55, SKL-HIDCA-2022-2, SKL-HIDCA-2022-3 and SKL-HIDCA-2022-GJ1), Xinjiang Medical University/State Key Laboratory of Pathogenesis, Prevention and Treatment of High Incidence Diseases in Central Cultivation Project of National Science Foundation for Outstanding Young People (No. xyd2021Y005), and Xinjiang Autonomous Region Health Commission, Young Scientific and Technological Talents Project (No. WJWJ202012).

Notes and references

1 A. Getaneh, B. Tegene and T. Belachew, *BMC Public Health*, 2021, **21**, 775.
2 M. Paskeh, S. Mirzaei, M. H. Gholami, A. Zarrabi, A. Zabolian, M. Hashemi, K. Hushmandi, M. Ashrafizadeh, A. R. Aref and S. Samarghandian, *Biomed. Pharmacother.*, 2021, **144**, 112335.
3 Y. Wu, Y. Chong, C. Han, K. Kang, Z. Liu and F. Zhang, *Ann. Transl. Med.*, 2021, **9**, 1375.
4 P. Xu and F. Liang, *Int. J. Nanomed.*, 2020, **15**, 9159–9180.

5 Z. Lv, S. He, Y. Wang and X. Zhu, *Adv. Healthcare Mater.*, 2021, **10**, e2001806.
6 J. Sun, F. Xing, J. Braun, F. Traub, P. M. Rommens, Z. Xiang and U. Ritz, *Int. J. Mol. Sci.*, 2021, **22**, 11354.
7 L. Zhao, X. Zhang, X. Wang, X. Guan, W. Zhang and J. Ma, *J. Nanobiotechnol.*, 2021, **19**, 335.
8 B. Zhou, C. Yin, Q. Feng, Y. Wu, X. Pan, C. Liu, J. Tian, S. Geng, K. Wang, J. Xing, Y. Cao, P. Shou, Z. Yu and A. Wu, *Nanoscale*, 2021, **13**, 19085–19097.
9 T. Qiu, Y. Lan, Z. Wei, Y. Zhang, Y. Lin, C. Tu, G. Mao, L. Zhang, B. Yang and J. Zhang, *Int. J. Nanomed.*, 2021, **16**, 2879–2896.
10 Z. Ke, A. Xie, J. Chen, Z. Zou, L. Shen, Y. Dai and D. Zou, *Biomater. Sci.*, 2020, **8**, 2481–2487.
11 T. Zheng, W. Wang, F. Wu, M. Zhang, J. Shen and Y. Sun, *Theranostics*, 2019, **9**, 5035–5048.
12 X. Zhang, L. Luo, L. Li, Y. He, W. Cao, H. Liu, K. Niu and D. Gao, *Nanomedicine*, 2019, **15**, 142–152.
13 J. Yu, S. Liu, Y. Wang, X. He, Q. Zhang, Y. Qi, D. Zhou, Z. Xie, X. Li and Y. Huang, *Bioact. Mater.*, 2021, **7**, 389–400.
14 Z. H. Feng, Z. T. Li, S. Zhang, J. R. Wang, Z. Y. Li, M. Q. Xu, H. Li, S. Q. Zhang, G. X. Wang, A. Liao and X. Zhang, *Acta Biomater.*, 2021, **136**, 495–507.
15 Y. Wang, F. Zhang, H. Lin and F. Qu, *ACS Appl. Mater. Interfaces*, 2019, **11**, 43964–43975.
16 C. W. Ting, Y. H. Chou, S. Y. Huang and W. H. Chiang, *Colloids Surf., B*, 2021, **208**, 112048.
17 L. Zhu, J. Chen, T. Yan, G. Alimu, X. Zhang, S. Chen, M. Aimaiti, R. Ma and N. Alifu, *J. Biophotonics*, 2021, **14**, e202100117.
18 B. Navyatha and S. Nara, *Nanobiomedicine*, 2021, **8**, 18495435211053945.
19 S. Choi, S. H. Lee, S. Park, S. H. Park, C. Park and J. Key, *Yonsei Med. J.*, 2021, **62**, 1042–1051.
20 E. D. Cosco, I. Lim and E. M. Sletten, *ChemPhotoChem*, 2021, **5**, 727–734.
21 A. Nanashima, M. Hiyoshi, N. Imamura, K. Yano, T. Hamada and K. Kai, *Curr. Oncol.*, 2021, **28**, 4067–4079.
22 B. S. Dash, S. Das and J. P. Chen, *Int. J. Mol. Sci.*, 2021, **22**, 6658.
23 L. Wu, S. Fang, S. Shi, J. Deng, B. Liu and L. Cai, *Biomacromolecules*, 2013, **14**, 3027–3033.
24 R. Ma, N. Alifu, Z. Du, S. Chen, Y. Heng, J. Wang, L. Zhu, C. Ma and X. Zhang, *Int. J. Nanomed.*, 2021, **16**, 4847–4861.
25 S. H. Chen, L. J. Zhu, Z. Du, R. Ma, T. Yan, G. Alimu, X. L. Zhang, N. Alifu and C. Ma, *RSC Adv.*, 2021, **11**, 20850–20858.
26 A. K. Srivastava, S. R. Choudhury and S. Karmakar, *ACS Appl. Mater. Interfaces*, 2020, **12**, 5658–5670.
27 L. Wang, L. Hui and W. Su, *Carbohydr. Polym.*, 2022, **275**, 118710.
28 F. Tian, X. Zhong, J. Zhao, Y. Gu, Y. Fan, F. Shi, Y. Zhang, Y. Tan, W. Chen, C. Yi and M. Yang, *J. Mater. Chem. B*, 2021, **9**, 9358–9369.
29 Y. Lu, X. Zhang, X. Hou, M. Feng, Z. Cao and J. Liu, *Nanoscale*, 2021, **13**, 17822–17836.
30 J. Yao, F. Zheng, F. Yang, C. Yao, J. Xing, Z. Li, S. Sun, J. Chen, X. Xu, Y. Cao, N. Hampp and A. Wu, *Biomater. Sci.*, 2021, **9**, 7591–7602.
31 Y. Zhou, B. Lin, K. Li, Y. Zhao, Z. Sun, C. He and R. K. Jha, *Front. Oncol.*, 2021, **11**, 750807.
32 Z. Jin, Y. Dun, L. Xie, W. Jiang, X. Sun, P. Hu, S. Zheng and Y. Yu, *Colloids Surf., B*, 2021, **208**, 112107.
33 J. Wang, Y. Guo, J. Hu, W. Li, Y. Kang, Y. Cao and H. Liu, *Langmuir*, 2018, **34**, 9516–9524.
34 X. Lin, Y. Cao, J. Li, D. Zheng, S. Lan, Y. Xue, F. Yu, M. Wu and X. Zhu, *Biomater. Sci.*, 2019, **7**, 2996–3006.
35 M. Tchouagué, M. Grondin, A. Glory and D. Averill-Bates, *Chem.-Biol. Interact.*, 2019, **310**, 108717.
36 J. Shao, R. Liang, D. Ding, X. Zheng, X. Zhu, S. Hu, H. Wei and B. Wei, *Int. J. Nanomed.*, 2021, **16**, 2897–2915.
37 D. Zhang, J. Zhang, Q. Li, H. L. Tian, N. Zhang and Z. H. Li, *ACS Appl. Mater. Interfaces*, 2018, **15**, 4431–4440.
38 Y. Liu, K. Ai, J. Liu, M. Deng, Y. He and L. Lu, *Adv. Mater.*, 2013, **25**, 1353–1359.
39 X. Sun, G. He, C. Xiong, C. Wang, X. Lian, L. Hu, Z. Li, S. J. Dalgarno, Y. W. Yang and J. Tian, *ACS Appl. Mater. Interfaces*, 2021, **13**, 3679–3693.
40 H. Yi, W. Lu, F. Liu, G. Zhang, F. Xie, W. Liu, L. Wang, W. Zhou and Z. Cheng, *J. Nanobiotechnol.*, 2021, **19**, 134.
41 Z. Shi, C. Chu, Y. Zhang, Z. Su, H. Lin, X. Pang, X. Wang, G. Liu and W. Li, *J. Biomed. Nanotechnol.*, 2018, **14**, 1934–1943.
42 Q. Hu, K. Wang and L. Qiu, *Colloids Surf., B*, 2021, **197**, 111372.
43 S. Wilhelm, A. J. Tavares, Q. Dai, S. Ohta, J. Audet and H. F. Dvorak, *Nat. Rev. Mater.*, 2016, **1**, 16014.